Research Article

An Intravital Multiphoton Microscopy Model for visualization of tumor cell dissemination and lymphatic vasculature

Katharina Eder[1*], Steffen Dietzel[2], Ulrich Harreus[3], Brigitte Mack[1], Manuel Guhlich [4], Carola Eggert[1], Alexander Berghaus[1], Olivier Gires[1], Martin Canis[5]

[1] Department of Oto-Rhino-Laryngology, Head-and-Neck-Surgery, Ludwig-Maximilians-University Munich, Germany;
[2] Walter Brendel Centre of Experimental Medicine, Ludwig-Maximilians-University Munich, Germany;
[3] Department of Otolaryngology / Head-and-Neck-Surgery, EVK Duesseldorf, Germany;
[4] Department of Radiotherapy and Radiation Oncology, Georg-August-University Göttingen, Germany;
[5] Department of Oto-Rhino-Laryngology, Head-and-Neck-Surgery, Georg-August-University Göttingen, Germany.

Abstract

Tumor metastasis and its impact on the organism are the main causes of death in patients with squamous cell carcinoma of the head and neck region. The presence of metastasis at the time of diagnosis represents a negative prognostic parameter of overall survival and correlates with a 50 % mean reduction of life expectancy, independent of tumor size. The potential for metastasis depends on factors such as the proliferation rate, neoangiogenesis and invasive capacity in intact tissue structures. Many aspects of the molecular mechanisms and supportive factors are not understood. To allow the investigation of such factors, we developed an intravital mouse model for the visualization of tumor cell proliferation, dissemination and lymphatic vasculature by multiphoton microscopy. This technology offers deep tissue penetration, low phototoxicity, superior image contrast, and four-dimensional resolution for investigations at the single cell level in a physiological setting. The human oral cancer cell line OSC-19 was transfected with turbo-red fluorescent protein and implanted in murine pinna. Lymphatic structures were labeled with a deep red-labeled antibody specific for lymphatic vessel endothelial receptor-1. In future research, this model might serve as a tool to gain deeper insights in surface molecules involved in lymphatic metastasis as well as other molecular mechanisms of metastasis and tumor cell migration.

Keywords: Multiphoton microscopy model, OSC-19 tumor model, Lymphatic metastasis, Tumor cell migration, Head and neck cancer.

Introduction

Evidence of lymphatic spread is one of the most important prognostic factors for patients with head and neck squamous cell carcinoma (HNSCC) because overall survival can be reduced by more than 50 % given the presence of lymph node metastases, independently of primary tumor size (1, 2). The lymphatic system therefore plays a major role as a route of circulation and dissemination, enabling cancer cells to circulate and metastasize into potentially more than 400 lymph nodes in the cervical region (3). The invasion of cancer cells from the primary tumor into the surrounding tissue is a critical step that requires increased cell mobility. Moreover,

[*] **Corresponding author**: Katharina Eder, MD, Department of Oto-Rhino-Laryngology, Head-and-Neck-Surgery, Ludwig-Maximilians-University, Marchioninistr. 15, 81377 Munich, Germany. Email: Katharina.Eder@med.uni-muenchen.de, phone: +49 (89) 4400-73892, fax: +49 (89) 4400 76892
Citation: Eder K, et al. An Intravital Multiphoton Microscopy Model for visualization of tumor cell dissemination and lymphatic vasculature. Cancer Research Frontiers. 2015 Apr; 1(2): 200-207. doi: 10.17980/2015.200

Competing Interests: The authors declare that they have no competing interests.
Received October 31, 2014; Revised December 24, 2014; Accepted January 28, 2015.

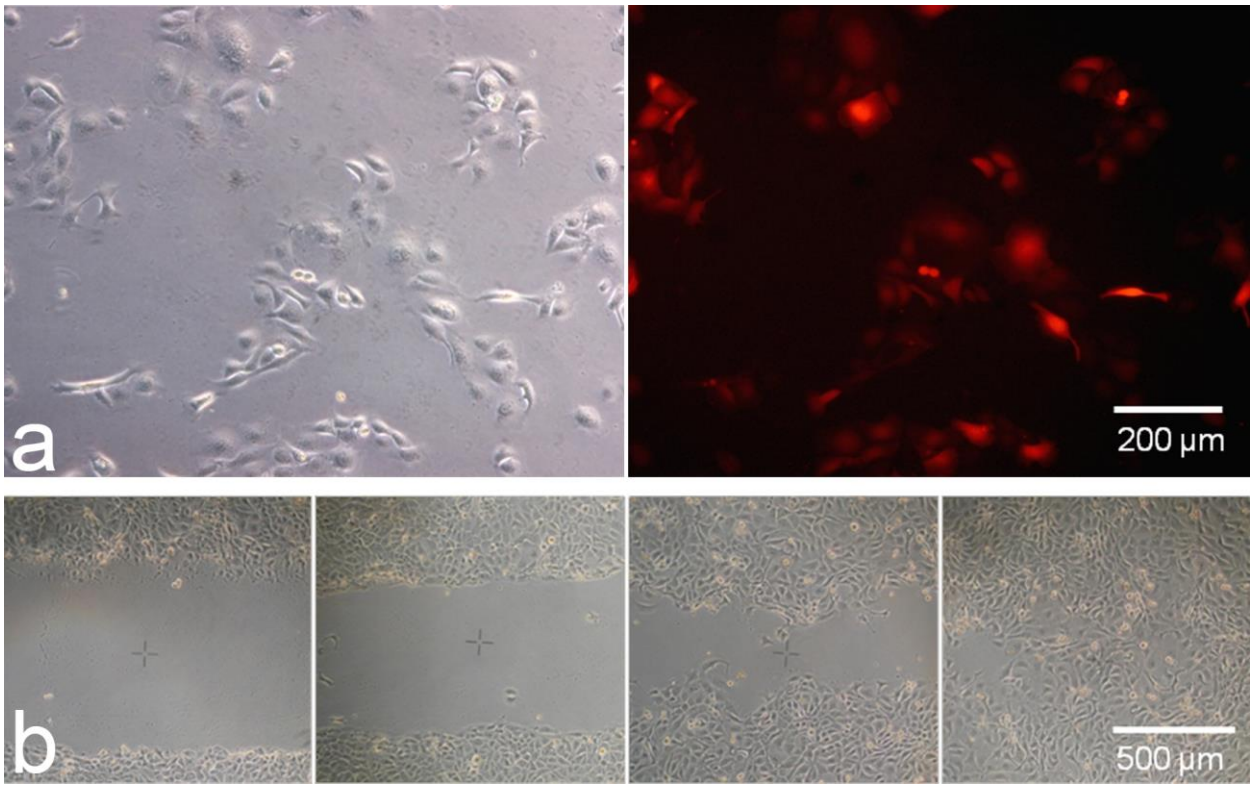

Figure 1. Labeling and migration capacity of OSC-19 tumor cells

(a) Comparison of phase contrast (left) and fluorescence microscopy (right) of OSC-19 cells lentivirally transfected with tRFP. While the intensity varied, nearly all cells provided a red fluorescent signal
(b) In a Scratch Wound Healing Assay a monolayer of OSC-19 cells was scratched with a sterile 1 ml pipette tip and observed every 4 hours. After 12 hours, the scratch was nearly closed.

to invade the lymphatic vessels, tumor cells typically must acquire the ability to degrade the extracellular matrix (ECM), survive in lymphatic circulation, extravasate out of vessels, settle and undergo sustained growth in lymph nodes (4). Until now, the details of the processes of lymphatic metastasis remained poorly understood, and due to the relative lack of efficient and objective methods, research on lymphatic metastases lags far behind that on hematogenous dissemination. Recently, multiphoton laser scanning microscopy (MPM) has provided insight into the mechanisms of hematogenous metastatic behavior of diverse entities such as breast or brain cancer (5). MPM uses longer wavelengths enabling a deeper penetration into tissue up to hundreds of µm, depending on the organ and model. This technique allows for *in vivo* imaging with four-dimensional (4D) resolution at the single cell level and for the visualization of the ECM through the use of second harmonic generation (SHG) phenomenon, a process that visualizes collagen without labeling (6-8). The aim of the present study was to establish an *in vivo* mouse model for visualization of tumor cell dissemination and peritumoral lymphatic tissue in a physiological setting by MPM.

Materials and Methods

Materials

Animals. Male adult NOD/SCID mice (6-8 weeks) were obtained from Charles River (Sulzfeld, Germany) and used at a body weight of 25-30 g. Animals were kept under pathogen-free conditions on standard laboratory chow and sterile water *ad libitum*. All experimental procedures were performed in compliance with the German legislation for animal experimentation and approved by the local government authorities (Regierung von Oberbayern; animal license no.: 55.2-1-54-2531-172-09)

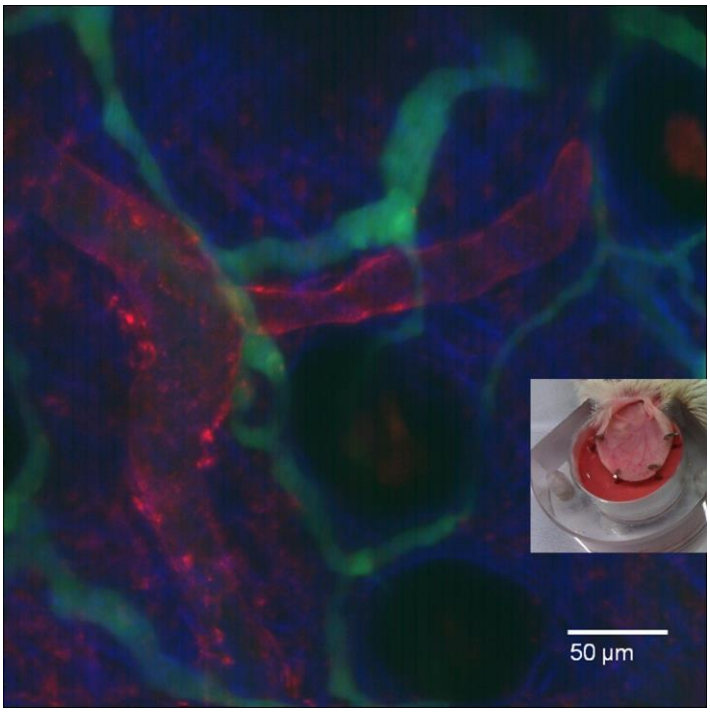

Figure 2. Multiphoton microscopy in the mouse pinna

This projection of 41 images with an axial Z-step size of 1 µm shows the lymphatic vasculature labeled with a subcutaneous injection of anti-mouse lymphatic vessel endothelial hyaluronan receptor-1 **(**Lyve-1) antibody coupled to eFluor® 660 in red and blood vessels labeled by intravenous injection of high-molecular FITC-dextran in green. Second harmonic generation (blue) highlights the connective tissue of the mouse pinna. This signal originates from the upper parts of the image stack, whereas the fluorescent signal indicates vessels from deeper parts of the image stack. Hair roots appear as black space. The mouse pinna was immobilized by surgical clips on a custom-built stage to allow investigation with a water immersion objective while maintaining physiological temperature (see inset).

Cell line and transfection. The human tongue cancer cell line OSC-19 was purchased from the Japanese Collection of Research Bioresources (JCRB) and cultured in Dulbecco's Modified Eagle Medium (DMEM)/Ham's F12 Medium (Gibco®) supplied with 10 % fetal calf serum (FCS) (Biochrom AG, Heidelberg, Germany) and 1 % penicillin/streptomycin. Cells were held in a 5 % CO_2 atmosphere at 37 °C and lentivirally transduced to express turbo-red fluorescent protein (tRFP) (Sirion Biotech, Planegg-Martinsried, Germany). tRFP has excitation/emission maxima of 553/574 nm, respectively. Cells were transduced using LV-Ubiqc-tRFP-IRES-Neo-vector with a multiplicity of infection (MOI) of 5. Selection of stably transfected cells was performed by adding 0.25 mg/ml G418 (Sigma-Aldrich, Munich, Germany) after 72 hours and culturing until all cells in the non-transfected controls died. tRFP transfection was confirmed by fluorescence microscopy. Cells were cultured with half the above-mentioned concentration of G418 and frequently evaluated for fluorescence.

Fluorophores. Lymph vessels were visualized using anti-mouse lymphatic vessel endothelial hyaluronan receptor-1 **(**Lyve-1) antibody coupled to eFluor® 660 (eBioscience, Frankfurt, Germany). The antibody-fluorophore conjugate was administered 24 hours prior to the multiphoton experiment by 2-3 microscopic peritumoral injections of 1-5 µl each at a concentration of 0.05 mg/ml subcutaneously into the pinna of the mouse using a 1 ml syringe (BD Micro-Fine^{TM}, Heidelberg, Deutschland). Fluorescein isothiocyanate (FITC)-labeled dextran (molecular weight 500,000; 0.05-0.1 ml of a 4 % solution in 0.9 % NaCl; Sigma, Deisenhofen, Germany) was injected intravenously as a plasma marker to visualize the vasculature.

Experimental Procedure

Cell counting and motility assay. In vitro experiments were performed to characterize the transfectants and to show proliferation compared to the wild type cells. Cell numbers were assessed upon trypan blue exclusion assay in Neubauer counting chambers. A scratch wound healing assay was used to detect cell migration. For this assay, homogeneous single-cell suspensions were added to six-well plates (2×10^5 cells/well) and cultured with 1 % FCS for 8 hours to a density of 80 %. Gently and slowly, the monolayer was scratched with a sterile 1 ml pipette tip across the center of the well in a straight line to generate a wound in the confluent cell monolayer. Thereafter, wells were washed 3 times with PBS, and 3 random sections of 6 scratches were marked at the rear side of the well. Pictures were taken at 4, 8, 12, 16 and 20 hours after the scratch under an Axiovert 25 microscope (Zeiss, Jena, Germany) with a Samsung WB750 camera (Samsung, Schwalbach, Germany). Image J software (9) was used to calculate the gap area and length of the scratch. The migration

velocity was calculated independently for all 4-hour-intervals until the gap was closed and is shown as an overall mean. Statistics were performed in Excel (Microsoft, Redmond, WA, USA).

Tumor cell implantation. OSC-19 cells were cultured as described above. First, $5x10^6$ cells were suspended in 50 µl medium/matrigel mixture with a ratio of 1:1 (BD Biosciences, Billerica, MA, USA). Then, 5-10 µl of cells were injected in the right pinna of 4 mice using a microfine syringe with a needle that was 0.3 mm in size and 8 mm in length (BD Micro-Fine™, Heidelberg, Germany) under observation with a stereomicroscope. Tumor growth and size were checked at day 3, 5, 6 and 7.

MPM setup. MPM was performed on a commercial system from LaVision BioTec (Bielefeld, Germany) described in detail elsewhere (10). An Olympus XLUMPlanFl 20 /0.95-WI objective (numerical aperture NA=0.95) and an optical parametric oscillator-generated excitation beam at λ = 1140 nm were used (Chamelon OPO pumped by a Chameleon Ultra II, both from Coherent, Dieburg, Germany). Laser power at 1140 nm was set between 110 and 145 mW, as measured behind the objective. While this power might cause significant damage, e.g., at 800 nm, the reduced absorption of longer wavelengths allows the application of even higher powers at the selected wavelength without detectable damage to the tissue. Dwell time per pixel was approximately 2 µs according to $I=16*P_{av}*NA^2/(R*W*\pi*\lambda^2)$ (11) with P_{av} = average Power 125 mW, R = repetition rate 80 MHz, W = width of pulse 200 fs, the latter two values taken from the data sheet of the OPO manufacturer, theoretical peak irradiance I was calculated as $2.7x10^{12}$ W/cm^2. This can be regarded as an upper limit estimate, since actual peak irradiance is decreased by scattering in the tissue and decreased optical resolution, introduced for example by refraction index mismatch of the tissue. The SHG signal from collagen at 570 nm was strong in the 580/60 nm channel, and tRFP signals were therefore recorded in the 624/40 nm channel. Lyve-1 staining was visualized at 665/60 nm and FITC was detected at 525/50 nm. All signals were recorded with backward (epi) detection. Hamamatsu H6780-20 photomultiplier tubes were used for all channels. Tumor localization in the sample before multiphoton investigation was performed by conventional epifluorescence microscopy with a Cy-3 filter.

MPM Protocol. At day 7 after tumor implantation, mice were anesthetized (intraperitoneal injection of 75.0 mg/kg body weight ketamine; 5.0 mg/kg body weight xylazine) and placed on a small custom-built plate allowing immobilization of the pinna by surgical clips. Body temperature was controlled constantly. The edge of the tumor was localized by epifluorescence microscopy (see above). Next, Z-stacks of up to 100 µm depth were taken at an area of up to 400x400 µm (966x966 px) with a repetition rate of 400 Hz at regions of colocalization of the tumor and lymphatics. After the experiment, mice were euthanized by intraperitoneal injection of phenobarbital (3 ml/kg b.w.). Images were processed by Fiji software, an ImageJ derivative (12).

Results and Discussion

The metastasis of head and neck cancer is linked to tumor invasion via the lymphatics and represents a major unsolved challenge in therapeutic management because it tightly correlates with a high risk for reduced long-term survival (2). Despite the clinical importance of lymphatic metastases in head and neck cancer, details of the processes and the underlying molecular mechanisms remain poorly understood. Previous studies have been conducted *in vitro* and *in vivo* to experimentally explore lymphangiogenesis using lymphatic endothelial cells and tumor cells in invasion assays (13, 14). However, animal models are especially unique in their ability to recapitulate the *in vivo* situation, including the tumor micro-environment. Mouse models of oral cancer have been developed to facilitate the study of factors that impact invasion and serve as a model for anti-tumor therapy (15). In these systems, visualization of disseminated tumor cells has been conducted primarily *ex vivo* (16) by conventional histology (15) or with *in vivo* bioluminescent methods (17). A primary drawback of these methods is the inherent inability to accurately visualize and quantify early tumor cell invasion arising from the primary site in three dimensions, in a physiological setting and at the single cell level. In recent years, MPM has been established and has been shown to have several technical advantages over conventional single-photon techniques (18). Compared to single-photon confocal microscopy, MPM allows for deeper penetration into tissue; avoids a pinhole aperture for confocality, resulting in greater efficiency of fluorescent light; reduces bleaching of the fluorophores; and visualizes the ECM by second harmonic scattering (19). MPM has been used in several studies for *in vivo* investigations of the tumor growth and metastatic behavior of glioblastoma (5), breast cancer (20) and other entities (21). For head and neck cancer, an orthotopic tongue carcinoma *ex vivo* mouse model was recently published (16); however, *in vivo* animal models are

still missing. This absence may be explained by the fact that, compared to other entities, orthotopic head and neck tumors are difficult to access with MPM because immobilization of the soft tissue is almost impossible due to the inherent movements associated with the breath and heartbeat. However, heterotopic *in vivo* models have also not been published.

Therefore, the major aim of the present study was to establish and technically describe a heterotopic *in vivo* head and neck cancer mouse model to visualize tumor cell proliferation, early cell dissemination and lymphatic vasculature by MPM. For this aim, an intravital MPM model for the visualization of tumor cells, lymphatic tissue, capillary vasculature and ECM in the mouse pinna was established.

Injection of OSC-19 cells, a human oral cancer cell line, into the tongue causes reliable tumor growth and metastasis formation (22). Therefore, we transduced OSC-19 cells with tRFP **(Figure 1A)**. In an initial set of *in vitro* experiments, the proliferation and migration capacity of transfected OSC-19 cells was assessed using a scratch wound healing assay. After scratching a confluent layer of OSC-19 cells, the velocity of wound closure was addressed over time. OSC-19 cells were determined to be highly motile, and the mean migration velocity was 25.7 µm/h (SD 7.88, n=32). Figure 1B shows a scratch wound healing assay demonstrating that a scratch of a 1 ml pipette tip was nearly closed after 12 hours (**Figure 1B**). Thus, transfected OSC-19 cells were comparable to the wild type and considered to be appropriate for MPM investigations. In the first *in vivo* experiment, we investigated the possibility of visualizing the lymphatic system in the pinna of control mice. After immobilization of the pinna by surgical clips, anti-mouse Lyve-1 antibodies were injected subcutaneously. For comparison, we visualized the blood vessels by intravenous administration of FITC-dextran. We indeed could detect lymphatic vessels together with blood capillaries and the ECM, with the latter detected by SHG (**Figure 2**; n=3). In our model, the ECM can be visualized by SHG as a dense network with a maximum depth of 60 µm below the epidermis. First, it is commonly used as a reference point. When looking at migrating single cells, visualizing the ECM allows retracking of the imaged areas over time (23, 24). Additionally, it serves as a reference point when examining the extra- or intravasation of cells (25). Secondly, the ECM itself might be of interest when investigating mechanisms of invasion by tumor cells. For example, *Wolf et al.* showed that the degradation of ECM is not always necessary for tumor cells to invade, but tumor cells can switch from a mesenchymal mode of migration to an amoeboid mode, leaving collagen intact and squeezing through gaps between collagen fibers (26, 27). We did not observe any collagen fluorescence with our excitation wavelength of 1140 nm. This is in accordance with the literature showing that two-photon excitation fluorescence of collagen is limited to excitation wavelengths shorter than 800 nm (28).

The maximum imaging depth we obtained was ~110 µm from the outermost surface. This value depends on the amount of scattering by the hair and epidermis. High quality imaging was usually possible up to an imaging depth of ~80 µm. This is in line with the literature. Ng *et al.* describe similar penetration depths when studying dermal dendritic cells in the mouse pinna (29).

In the second *in vivo* experiment, OSC-19 cells transduced with tRFP were injected subcutaneously into the pinna of mice (n=4). Tumor growth was observed over seven days. Macroscopic tumor growth was visible after a mean duration of 5 ± 2 days after implantation in all four mice. Tumors appeared as flat round indurations up to a maximum of 4 mm in diameter at day seven (**Figures 3A** and **3B**).

Subcutaneous injection of Lyve-1 antibody in mice with tRFP OSC-19 tumors allowed the *in vivo* covisualization of transfected cells next to the lymphatic vasculature by MPM (**Figures 3C, 3D and 3E**).

At present, the combination of the immobilized pinna with tumor growth of a highly motile cell line allows for physiological visualization of peritumoral cell dissemination and lymphatic vasculature without any further surgical manipulation. In the future, this model might be able to give further insights in cell migration and surface molecules involved in early lymphatic metastasis.

Acknowledgments

This study was supported by Münchener Medizinische Wochenschrift, the BioImaging Network of the Ludwig-Maximilians-Universität München and the Excellence Initiative of the Deutsche Forschungsgemeinschaft and the Bundesministerium für Bildung und Forschung.

Abbreviations

HNSCC	Head and Neck Squamous Cell Carcinoma
ECM	Extracellular Matrix

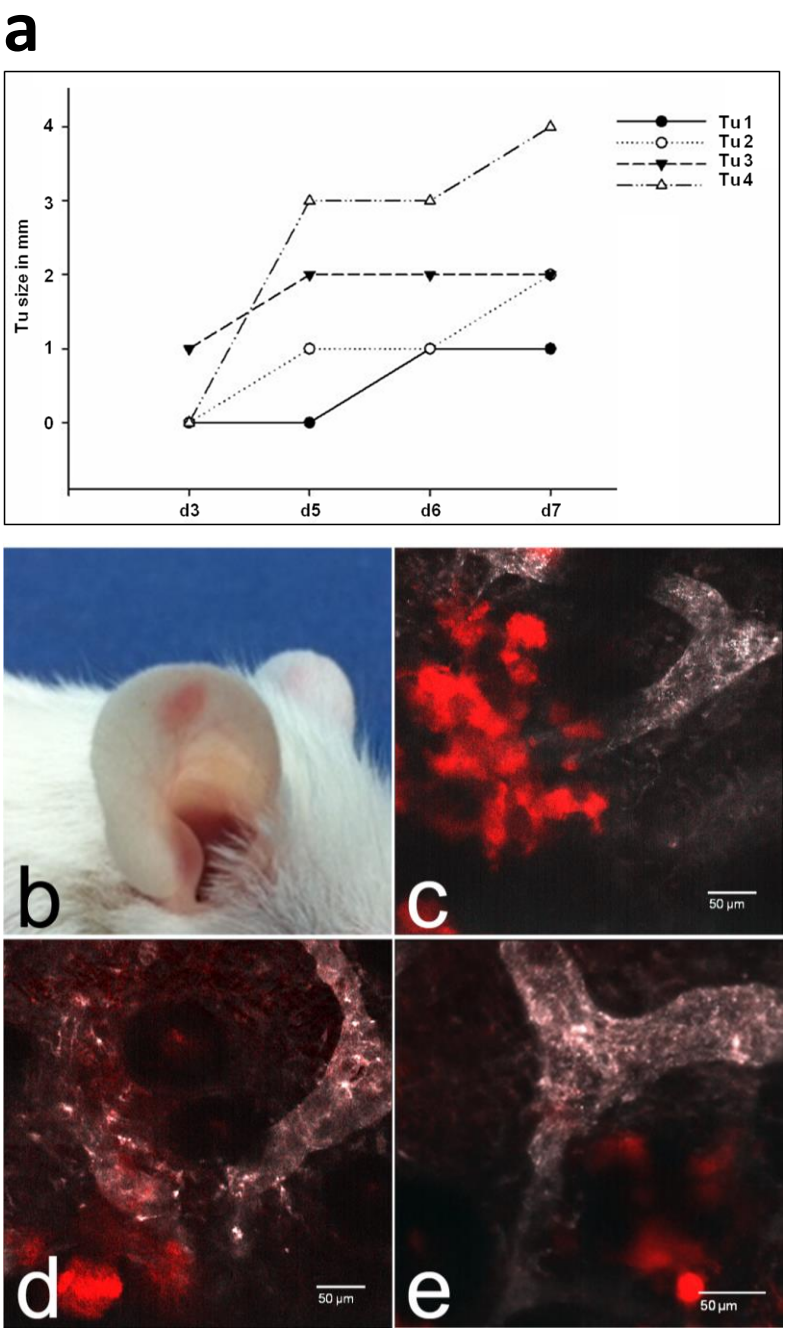

Figure 3. Tumor growth and Multiphoton imaging of OSC-19 tumor

(a) Tumor (Tu) growth in 4 mice in mm over time: OSC-19 tumor cells were subcutaneously injected in the mouse pinna and observed over 7 days. After a mean duration of 5 ±2 days macroscopic tumor growth was visible and measured.
(b) Seven days before OSC-19 tumor cells were subcutaneously injected in the right pinna of the mouse, leading to macroscopic tumor growth.
(c) and (d) Single Multiphoton Microscopy XY-images of tumor cells at the edge of the OSC-19 tumor are shown in close relation to the lymphatic vasculature. OSC-19 cells were injected 7 days prior to imaging. Tumor cells are shown in red, labeled with tRFP. Lymphatic vessels are shown in a pinkish-white color, labeled with anti-mouse lymphatic vessel endothelial hyaluronan receptor-1 (Lyve-1) antibody coupled to eFluor® 660.
(e) A Z-projection (Z=26 µm, 2 µm axial step size) of Multiphoton microscopy images shows OSC-19 tumor cells and lymphatic vasculature 7 days after the implantation of tumor cells. Lymphatic vessels are shown in a pinkish-white color, labeled with anti-mouse lymphatic vessel endothelial hyaluronan receptor-1 (Lyve-1) antibody coupled to eFluor® 660. Tumor cells are shown in red, labeled with tRFP.

MPM	Multiphoton Laser Scanning Microscopy
4D	Four-Dimensional
SHG	Second Harmonic Generation
DMEM	Dulbecco's Modified Eagle Medium
FCS	Fetal Calf Serum
tRFP	Turbo-Red Fluorescent Protein
MOI	Multiplicity of Infection
Lyve-1	Lymphatic Vessel Endothelial Hyaluronan Receptor-1
FITC	Fluorescein Isothiocyanate

References

1. Lang S, Wollenberg B, Dellian M, Steuer-Vogt MK, Schwenzer K, Sautier W, et al. [Clinical and epidemiological data of patients with malignomas of the head and neck]. Laryngorhinootologie. 2002 Jul;81(7):499-508. DOI: 10.1055/s-2002-33285.

2. Mehanna H, West CM, Nutting C, Paleri V. Head and neck cancer--Part 2: Treatment and prognostic factors. BMJ. 2010;341:c4690. DOI: 10.1136/bmj.c4690.

3. Wang Y, Ow TJ, Myers JN. Pathways for cervical metastasis in malignant neoplasms of the head and neck region. Clin Anat. 2012 Jan;25(1):54-71. DOI: 10.1002/ca.21249.
4. Zhang Q, Shi S, Yen Y, Brown J, Ta JQ, Le AD. A subpopulation of CD133(+) cancer stem-like cells characterized in human oral squamous cell carcinoma confer resistance to chemotherapy. Cancer Lett. 2010 Mar 28;289(2):151-60. DOI: 10.1016/j.canlet.2009.08.010.
5. Kienast Y, von Baumgarten L, Fuhrmann M, Klinkert WE, Goldbrunner R, Herms J, et al. Real-time imaging reveals the single steps of brain metastasis formation. Nat Med. 2010 Jan;16(1):116-22. DOI: 10.1038/nm.2072.
6. Fine S, Hansen WP. Optical second harmonic generation in biological systems. Appl Opt. 1971 Oct 1;10(10):2350-3. DOI: 10.1364/AO.10.002350.
7. Zipfel WR, Williams RM, Christie R, Nikitin AY, Hyman BT, Webb WW. Live tissue intrinsic emission microscopy using multiphoton-excited native fluorescence and second harmonic generation. Proc Natl Acad Sci U S A. 2003 Jun 10;100(12):7075-80. DOI: 10.1073/pnas.0832308100.
8. Campagnola PJ, Millard AC, Terasaki M, Hoppe PE, Malone CJ, Mohler WA. Three-dimensional high-resolution second-harmonic generation imaging of endogenous structural proteins in biological tissues. Biophys J. 2002 Jan;82(1 Pt 1):493-508. DOI: 10.1016/S0006-3495(02)75414-3.
9. Schneider CA, Rasband WS, Eliceiri KW. NIH Image to ImageJ: 25 years of image analysis. Nat Methods. 2012 Jul;9(7):671-5.
10. Rehberg M, Krombach F, Pohl U, Dietzel S. Label-free 3D visualization of cellular and tissue structures in intact muscle with second and third harmonic generation microscopy. PLoS One. 2011;6(11):e28237. DOI: 10.1371/journal.pone.0028237.
11. Supatto W, Debarre D, Moulia B, Brouzes E, Martin JL, Farge E, et al. In vivo modulation of morphogenetic movements in Drosophila embryos with femtosecond laser pulses. Proc Natl Acad Sci U S A. 2005 Jan 25;102(4):1047-52. DOI: 10.1073/pnas.0405316102.
12. Schindelin J, Arganda-Carreras I, Frise E, Kaynig V, Longair M, Pietzsch T, et al. Fiji: an open-source platform for biological-image analysis. Nat Methods. 2012 Jul;9(7):676-82. DOI: 10.1038/nmeth.2019.
13. Karatzanis AD, Koudounarakis E, Papadakis I, Velegrakis G. Molecular pathways of lymphangiogenesis and lymph node metastasis in head and neck cancer. Eur Arch Otorhinolaryngol. 2012 Mar;269(3):731-7. DOI: 10.1007/s00405-011-1809-2.
14. Smith A, Teknos TN, Pan Q. Epithelial to mesenchymal transition in head and neck squamous cell carcinoma. Oral Oncol. 2013 Apr;49(4):287-92. DOI: 10.1016/j.oraloncology.2012.10.009.
15. Sano D, Myers JN. Xenograft models of head and neck cancers. Head Neck Oncol. 2009;1:32. DOI: 10.1186/1758-3284-1-32.
16. Gatesman Ammer A, Hayes KE, Martin KH, Zhang L, Spirou GA, Weed SA. Multi-photon imaging of tumor cell invasion in an orthotopic mouse model of oral squamous cell carcinoma. J Vis Exp. 2011 (53). DOI: 10.3791/2941.
17. Law JH, Whigham AS, Wirth PS, Liu D, Pham MQ, Vadivelu S, et al. Human-in-mouse modeling of primary head and neck squamous cell carcinoma. Laryngoscope. 2009 Dec;119(12):2315-23. DOI: 10.1002/lary.20607.
18. Gratton E, Barry NP, Beretta S, Celli A. Multiphoton fluorescence microscopy. Methods. 2001 Sep;25(1):103-10. DOI: 10.1006/meth.2001.1219.
19. Chen WL, Hu PS, Ghazaryan A, Chen SJ, Tsai TH, Dong CY. Quantitative analysis of multiphoton excitation autofluorescence and second harmonic generation imaging for medical diagnosis. Comput Med Imaging Graph. 2012 Oct;36(7):519-26. DOI: 10.1016/j.compmedimag.2012.06.003.
20. Bonapace L, Wyckoff J, Oertner T, Van Rheenen J, Junt T, Bentires-Alj M. If you don't look, you won't see: intravital multiphoton imaging of primary and metastatic breast cancer. J Mammary Gland Biol Neoplasia. 2012 Jun;17(2):125-9. DOI: 10.1007/s10911-012-9250-8.
21. Watson JM, Marion SL, Rice PF, Bentley DL, Besselsen DG, Utzinger U, et al. In vivo time-serial multi-modality optical imaging in a mouse model of ovarian tumorigenesis. Cancer Biol Ther. 2014 Jan;15(1):42-60. DOI: 10.4161/cbt.26605.
22. Kawashiri S, Kumagai S, Kojima K, Harada H, Nakagawa K, Yamamoto E. Reproduction of occult metastasis of head and neck cancer in nude mice. Clin Exp Metastasis. 1999 Jun;17(4):277-82.
23. Perentes JY, McKee TD, Ley CD, Mathiew H, Dawson M, Padera TP, et al. In vivo imaging of extracellular matrix remodeling by tumor-associated fibroblasts. Nat Methods. 2009 Feb;6(2):143-5. DOI: 10.1038/nmeth.1295.

24. Kimura H, Hayashi K, Yamauchi K, Yamamoto N, Tsuchiya H, Tomita K, et al. Real-time imaging of single cancer-cell dynamics of lung metastasis. J Cell Biochem. 2010 Jan 1;109(1):58-64. DOI: 10.1002/jcb.22379.
25. Hoeller C, Richardson SK, Ng LG, Valero T, Wysocka M, Rook AH, et al. In vivo imaging of cutaneous T-cell lymphoma migration to the skin. Cancer Res. 2009 Apr 1;69(7):2704-8. DOI: 10.1158/0008-5472.CAN-08-2891.
26. Wolf K, Mazo I, Leung H, Engelke K, von Andrian UH, Deryugina EI, et al. Compensation mechanism in tumor cell migration: mesenchymal-amoeboid transition after blocking of pericellular proteolysis. J Cell Biol. 2003 Jan 20;160(2):267-77. DOI: 10.1083/jcb.200209006.
27. Wolf K, Alexander S, Schacht V, Coussens LM, von Andrian UH, van Rheenen J, et al. Collagen-based cell migration models in vitro and in vivo. Semin Cell Dev Biol. 2009 Oct;20(8):931-41. DOI: 10.1016/j.semcdb.2009.08.005.
28. Zoumi A, Yeh A, Tromberg BJ. Imaging cells and extracellular matrix in vivo by using second-harmonic generation and two-photon excited fluorescence. Proc Natl Acad Sci U S A. 2002 Aug 20;99(17):11014-9. DOI: 10.1073/pnas.172368799.
29. Ng LG, Hsu A, Mandell MA, Roediger B, Hoeller C, Mrass P, et al. Migratory dermal dendritic cells act as rapid sensors of protozoan parasites. PLoS Pathog. 2008;4(11):e1000222. DOI: 10.1371/journal.ppat.1000222.